# Development of a Photo-Acoustic Trace Gas Sensor

**C. Kelly (1,2), J. Leis (1) and D. Buttsworth (1)**

(1) Faculty of Engineering and Surveying, University of Southern Queensland, Toowoomba, Australia
(2) Gas Detection Australia, Toowoomba, Australia

## ABSTRACT

The work presented in this paper addresses the problem of creating a low-cost, intrinsically safe, low-level gas sensor for mining and transportation applications. The system is to have no electrical connection to the remote sensor head, and as such relies on optical transmission via fibre. An integral component is the acoustically resonant chamber, which is excited by an appropriate laser excitation. The laser is modulated at the resonant frequency of the chamber to create periodic heating, causing expansion. This is followed by cooling and thus contraction, resulting in a periodic pressure wave. The pressure wave is amplified in the resonant chamber, and then measured using an optical microphone approach. This makes the sensor inherently safe, as there are no electronics at the sensor head nor electrical connections required. A particular challenge associated with this approach is the acoustic signal generation and extraction from very high levels of noise. This paper gives a background on the photo-acoustic method, and describes our approaches to the development of physical hardware and processing algorithms required for an embedded sensor.

## INTRODUCTION

The use of natural gas as a fuel is increasing, particularly because of its potential as a low-emissions energy source (EPA 2011). This has prompted increasing interest in the development of existing resources in Australia (Brown 2011). However the issue of leakage of natural gas, whose primary constituent is methane, is of considerable concern – not just in mining and processing areas, but also in urban distribution (McKenna 2011). Although statistically unlikely, the potential for damage and significant loss of life is a major concern (Polson & Klimasinska 2010). Of course, the hazard in the mining industry is ever-present, as evidenced by several tragic recent events (Andresen 2010, Stevenson 2010).

Conventional "off-line" gas sensing approaches require considerable laboratory expertise, and rely on gas chromatography or other means to determine the presence and/or concentration of gases. Such a dedicated laboratory is infeasible in many situations, and neither does it lend itself to real-time diagnostics.

Additionally, a safe system would require no electrical connection to the remote sensing head. This is particularly important where the possibility of explosive levels of methane gas arises, in transportation and mining in particular.

To address the safety aspect inherent in such situations, we are currently investigating the use of a near-real-time methane gas sensor using, primarily, the photo-acoustic approach. In essence, this technique utilizes acoustic resonance in a chamber as a proxy for the existence of certain species of gas. The acoustic resonance may be excited by a laser of appropriate wavelength. The laser beam itself is transported via fibre optic means, and thus there is no direct electrical connection into the area to be sensed.

The photo-acoustic approach is based on the fact that a light beam, suitably modulated, is able to induce acoustic resonances in an enclosed or semi-enclosed chamber. Provided the acoustic resonance is detected with an optical microphone, no direct electrical connection to the gas-sensing chamber is required. The system will employ low-cost near-infrared laser diodes as a radiation source, and one or more optical microphones as sensing elements. The use of advanced noise-reduction techniques will be pursued, to attempt to overcome one of the primary limitations of the technique: the very low level acoustic signals emanating from the gas-filled chamber.

The system envisaged in the current work involves:

(i) The use of photo-acoustic resonance rather than optical line absorption.
(ii) The use of optical fibre test signal input and sensing return.
(iii) The use of acoustic techniques to make it inherently safe.
(iv) The development of signal enhancement algorithms for reliable gas detection, using only the photo-acoustic signal.

Furthermore, because of the proposed deployment in mining, transportation and industrial environments, further aims are to:

(i) minimize the cost;
(ii) maximize the ease of deployment, and
(iii) minimize or eliminate manual calibration requirements.

## PHOTO-ACOUSTIC SENSING

The photo-acoustic effect is observed when light which is modulated at a certain frequency produces an acoustic output. In gases, the very small acoustic signal resulting from this modulation may be enhanced by the use of an acoustic resonator. Relaxation processes (collisions with other molecules) lead to local warming and thus thermal expansion, followed by cooling and contraction. The resulting acoustic or ultrasonic waves can be detected (Bageshwar 2011).

Multiple resonant cell designs will be analysed for their performance. The designs to be examined include a basic closed-end cylindrical resonator, a Helmholtz resonator with buffer

volumes and a quartz enhanced Photo-Acoustic (PA) resonator. Models for each design will be generated using a lumped acoustic parameter approach, which may be solved using an electrical circuit analogy.

The system will ideally employ low-cost near-infrared laser diodes as the excitation source, and one or more optical microphones as sensing elements. The use of advanced noise-reduction techniques will be pursued, in order overcome the problems inherent in very low signal levels.

The PA effect on solids was discovered by A. G. Bell in 1880. The PA effect on liquids and solids was discovered soon after. Because of equipment limitation, significant research into the PA effect wasn't pursued for a half a century. The development of PA systems didn't come back into mainstream research until the 1970's and 1980's with development of high quality and power lasers (Miklos, 2001).

Different resonant cell designs are being investigated such as cylindrical resonators by Riddle (2006), Rey (2004, 2008 and 2010), Schmid (2006), Tavakoli (2010) and Lui (2010), Helmholtz resonators by Schilt (2006) and Nordhaus (1981), quartz enhanced photo-acoustic spectroscopy by Kosterev (2005), multi-pass PA cells by Sigrist (2003 and 2004) and cavity ring down by Nagi (2006). Different excitation techniques have been investigated like dual excitation frequency by Rey (2008) and Sigrist (2010).Various arrangements have been employed, such as continuous-wave optical parametric oscillators by Ngai (2006). Research has also been performed into signal processing techniques applied to PA Spectroscopy (PAS) , for example using the Fast Fourier Transform (FFT) by Slezak (2002).

Riddle (2006) investigated some of the problems with Laser Photo-Acoustic Spectroscopy (LPAS) with impedance optimised microphone placement on the PA cell, where the signal output of the PA cell is degraded by placing the microphone in the centre of the resonant chamber. It was discovered that the microphone produced superior results signal off to one side of the centre due to an impedance mismatch, reducing the resonant qualities of the PA cell.

Bartlome (2009) investigated the difference between modulated and pulsed excitation of PA cells, finding that the pulsed excitation provides a larger and more discernable signal by a factor of $\pi/2$.

Schilt (2006) demonstrated that methane's relaxation time restricts the possible excitation frequency range, but found that the effect can be reduced by adding a catalysis gas to speed up the relaxation of the methane.

## Spectroscopy and photo-acoustic spectroscopy

Optical spectroscopy is fundamentally based upon two principles: that molecules only transition from one steady energy state to another, and the de Broglie theorem of wave-particle duality. These principles are joined by Einstein's quantum theory of radiation, which states that there are three types of transitions between two atomic steady states. These transitions are absorption, spontaneous emission and stimulated emission, as described by equation (1),

$$f_{ik} = \frac{E_k - E_i}{h} \quad (1)$$

where steady states $i$ and $k$, with energies $E_i$ and $E_k$ respectively, $f_{ik}$ is the frequency in $Hz$ of the radiation and $h$ is Plank's constant. Absorption transitions are when light is absorbed with the same energy as the difference between the steady states. Spontaneous emission is when the atom releases energy in the form of a photon with the same energy as the difference between two steady states. This is governed by probabilistic processes. Stimulated emission is when the atom will emit a photon when stimulated by another photon. The emitted photon will have the same frequency and wavelength as the one that stimulated it (L'vov, 1970).

This response to specific frequencies leads to resonant absorption lines as shown on Figures 1, 2 and 3 of the absorption spectra of methane ($CH_4$). Figure 1 shows the fundamental absorption lines at 3.3 $\mu m$ and the overtone of the resonant absorption lines at 2.3 $\mu m$ and 1.66 $\mu m$. The precise nature of the absorption lines of the 1.66 $\mu m$ $CH_4$ absorption spectrum is shown in Figure 2, except at 1.667 $\mu m$ where several absorption lines have blurred together. This occurs because the absorption lines are not perfectly thin and the overtones overlap.

It can be clearly seen in Figure 3, where only one absorption line is shown that the lines are broadened, this occurs by natural, Doppler and Lorentz broadening. Natural broadening is due to quantum mechanics were there is a degree of uncertainty, causing a statistical variation of the resonant frequency in and between atoms and molecules.

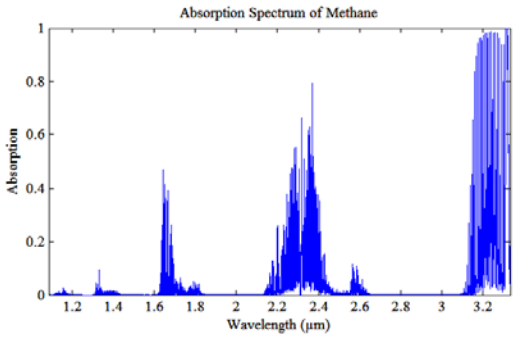


**Figure 1.** Absorption Spectrum of Methane, from $\lambda = 1\ \mu m$ to 3.3 $\mu m$, $l = 1\ m$ , $T = 296\ °K$, $C = 5\%$ and $P = 1\ atm$ (*Spectroscopy of Atmospheric Gases* 2011).

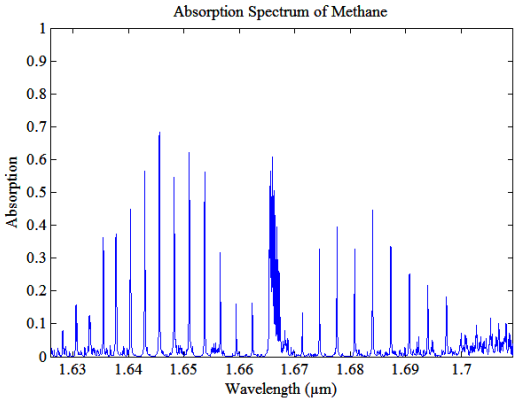


**Figure 2.** Absorption spectrum of methane, from $\lambda = 1.62\ \mu m$ to 1.71 $\mu m$, $l = 1\ m$ , $T = 296\ °K$, $C = 5\%$ and $P = 1\ atm$ (*Spectroscopy of Atmospheric Gases* 2011).

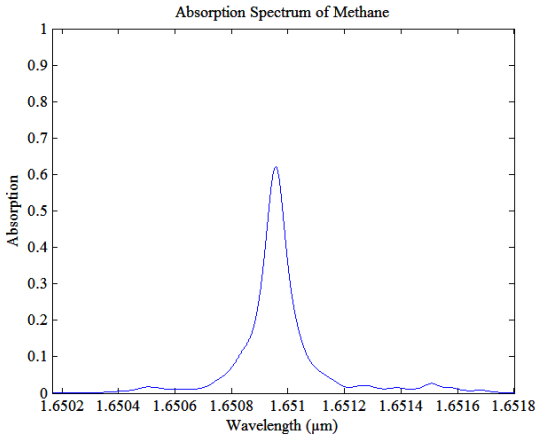


**Figure 3.** Absorption line of methane at $\lambda = 1650.95nm$, $l = 1\ m$ , $T = 296\ °K$, $C = 5\%$ and $P = 1\ atm$ (*Spectroscopy of Atmospheric Gases* 2011).

Natural broadening is the smallest broadening factor out of the three and can almost be neglected. Doppler broadening occurs because of the random thermal motion of atoms, where the Doppler Effect, described later in the paper, changes the resonant frequency of the atom/molecule with respect to the amplitude of the random thermal motion, causing the absorption lines to blur. Lorentz broadening is caused by the interaction between foreign atoms and molecules on the absorbing atoms and molecules. Lorentz broadening also shifts the resonate peak of the absorption line. With all broadening, the amplitude of the absorption lines are reduced and the integral of the absorption line is the same before and after broadening (Sasada, 1996) (L'vov, 1970).

The photo-acoustic effect in gases occurs as follows. The modulated or pulsed laser radiation gets absorbed. The substance becomes excited and relaxes back to its previous state via vibration and collisions. This energy is ideally completely transformed into heat. Heating causes expansion, a localised and transient density change. It cools contracting back to previous state. The density change causes a pressure wave as it normalises to the rest of the chamber. Inside a resonant chamber the periodic pressure wave reflects and is amplified forming standing waves, these are then detected by a microphone (Bialkowski, 1996).

The peak pressure change $|\delta P|$ in Pascals $(Pa)$ from the PA effect has been derived by Bialkowski (1996) for a single pulse as,

$$\delta P \propto \frac{\alpha \beta E_L}{C_p \tau^{3/2}} \sqrt{\frac{c}{r}} \tag{2}$$

where $\alpha$ is the absorption coefficient $(m^{-1})$, $\beta$ is the volume expansion coefficient $(K^{-1})$, $E_L$ is the excitation pulse energy $(J)$ or energy per cycle for modulated excitation, $C_p$ specific heat capacity $(Jkg^{-1}K^{-1})$, $c$ is the speed of sound $(ms^{-1})$ in the medium, $r$ is the radial distance $(m)$ between the transducer and the source and the pressure perturbation time $\tau$ $(s)$, is the root-mean-square of the relaxation times and the pulse or modulation width. The relaxation times may need an additional acoustic relaxation time $\tau_a$ if the excitation beam is large or the sample is already significantly heated, where $\tau_a = w/2c^2$ and $w$ is the radius $(m)$ of the beam used for sample excitation.

## Laser photo-acoustic systems

A general PA system consists of the excitation source, driving electronics, modulation electronics, PA cell, microphone, microphone preamp and filtering, and a form of either signal recovery or/and signal recording. Figure 4 shows a LPAS system setup using an optical microphone setup. The excitation source is a laser with either a very small output bandwidth, which is current modulated to cause a frequency shift in the laser, so that for only half the acoustic cycle the laser's output is absorbed. Alternatively, a higher output power laser with a larger output line width, which is modulated by a square wave off and on, or by an optical chopper. Modulation, signal recovery and signal recording electronics are implemented as parts of a larger Control System (CS) utilising Digital Signal Processing (DSP). The modulating electronics is a remotely controlled function generator. The signal recovery is performed by a Lock-In Amplifier (LIA), described later in the paper and the signal recording is performed by a master control unit.

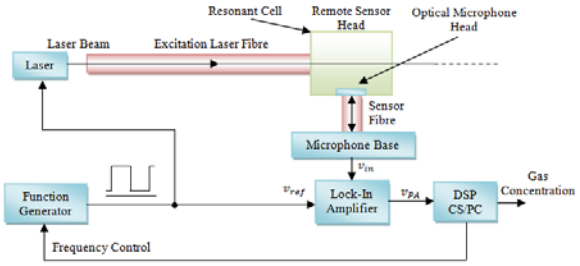


**Figure 4.** Photo-acoustic sensor principle of operation.

The function generator modulates the laser. The modulated excitation laser beam is sent to the PA cell via a fibre optic cable. If there is a gas or gases with absorption lines corresponding to the excitation laser's output, then acoustic waves will be developed. The resonant PA cell will amplify the signal and the optical microphone will detect it. The signal from the optical microphone is sent back the microphone base where it is transformed into an electrical signal, filtered and amplified enough for the LIA. The LIA recovers the actual PA signal from the noise by synchronous detection using the modulating wave form as the reference. The recovered PA signal is then passed to the CS for analysis, to derive the gas concentration.

## The lock-in amplifier

Since the acoustic signal realized from the resonant chamber is quite small, one of the key challenges is to amplify the signal enough to make a reliable measurement. We take advantage of the fact that we can periodically excite the acoustic cavity at a frequency of our choosing (within reason). Thus we judiciously choose the frequency to be well away from mains interference and other (predominantly odd) harmonics. The signal is detected from noise using a phase-sensitive or lock-in amplifier (Horowitz & Hill 1990, Preston & Deitz 1991). The acoustic signal is multiplied by the phase-delayed excitation signal, as depicted in Figure 5.

The phase delay is necessary to adjust for the delay in propagation through the system (fibre delay, acoustic delay, electronics and sampling). The multiplication is followed by a low-pass filter, thus effecting a form of correlator.

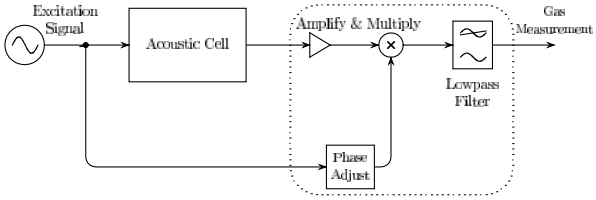


**Figure 5.** The single-source lock-in configuration. The laser is modulated at an acoustic frequency, and the light enters the resonant acoustic cell. The detected audio frequency is amplified, and multiplied by the phase-delayed audio excitation. The resultant is lowpass filtered and averaged to give the measurement of gas concentration.

One disadvantage to this approach is the necessity to tune the phase delay so as to maximize the detected output signal. This may be addressed by a slightly more complicated circuit arrangement as shown in Figure 6. This method uses not one, but two sinusoidal references in phase quadrature (that is, sine and cosine). Multiplication and lowpass filtering allows us to derive two signals I and Q, and from that we can calculate the measurement without the need for phase adjustment.

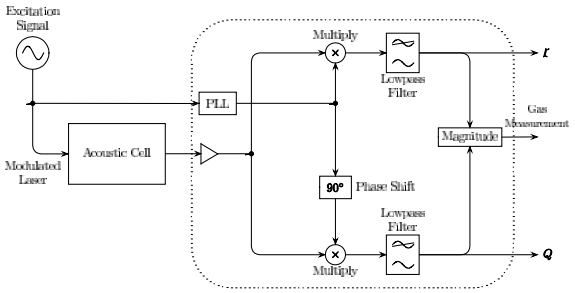


**Figure 6.** The enhanced lock-in configuration uses a single acoustic frequency, split into two components which are 90 degrees out of phase with each other. The Phase-Locked Loop (PLL) generates a signal of the same frequency and phase as the acoustic excitation, which is then multiplied by the detected acoustic signal from the photo-acoustic cell to give the in-phase component. Similarly, a quarter-wave delayed acoustic frequency signal is multiplied by the detected audio to give the quadrature output. These two signals are then lowpass filtered and converted into an equivalent indirect gas concentration measurement.

## DESIGN CONSIDERATIONS

The critical elements of the design of any LPAS system are the design of the resonant cell, selection of the laser and the quality of optics and electronics used. The general requirements of any LPAS system are well summarised by Miklos (2001),

i. good background suppression;
ii. good acoustic and vibration isolation;
iii. microphone with high response;
iv. low noise electronics; and
v. good electronic isolation (no ground loops, proper shielding).

Number five above is not as critical for this study because the gas sensor is going to be remote via optic fibre cables eliminating a large quantity of environmental noise to which an electrical sensor and communications would be susceptible to.

The focus of this paper is the design of the PA cell. The PA cell consists of the resonator, microphone, the laser entry and exit and the gas inlet and outlet as shown in Figure 4. The geometry of the resonator is the most critical aspect, followed by its construction and material. The resonator's geometry will define its resonant frequency $f_r$ in Hertz, acoustic resonator factor $F$ in $PaW^{-1}$ as defined by Tavakoli (2010) in equation (3) and the quality $Q$ (unitless) as defined by (Miklos, 2001) by equation (4),

$$F = \frac{|\delta P|}{\alpha P_L} \tag{3}$$

$$Q = \frac{2\pi \times Accumulated\ Energy}{Energy\ Lost\ Per\ Cycle} = \frac{f_r}{\Delta f} \tag{4}$$

where $|\delta P| = \delta P \cdot Q$ is the peak pressure change in Pascals $(Pa)$, $f_r$ is the resonant frequency in Hertz, $\Delta f$ is the Full Width at Half-Maximum (FWHM) which is measured as the difference in frequency between the points where the amplitude is $(1/2)$, with respect to power.

### Acoustic theory

The critical point of the design is the selection of base shape and the desired resonant mode. This paper investigates only in cylindrical tube and quartz based resonators. With a cylindrical tube there are three different resonant modes as shown in Figure 7. Longitudinal resonance is where the sound propagates from one end to the other. Azimuthal resonance is where the sound propagates around the circumference of the tube. Radial resonance is where the sound propagates from the centre of the cylinder to the outside of the tube.

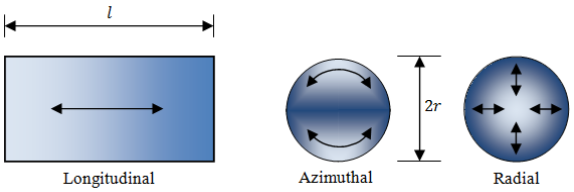


**Figure 7.** Resonant modes a cylindrical resonator (Apfel, 1998:76-78)

The resonant frequency for a cylindrical resonator for an ideal (lossless) case is given by equation (5) where $j, m, q$ are the mode numbers (non-negative integers) for the radial, azimuthal and longitudinal modes respectively, $f_{jmq}$ is the resonator frequency of the mode $jmq$, $c$ is the speed of sound $(ms^{-1})$, $\alpha_{jm}$ is the $j^{\text{th}}$ zero of the derivative of the $m^{\text{th}}$ Bessel function divided by $\pi$, $l$ is the length of the cylinder $(m)$ and $r$ is the radius of the cylinder $(m)$ (Miklos, 2001),

$$f_{jmq} = \frac{c}{2}\sqrt{\left(\frac{\alpha_{jm}}{r}\right)^2 + \left(\frac{q}{l}\right)^2} \tag{5}$$

The $jmq$ mode indices refer to the eigenvalues of the modes. This has implications for design. Typically only one mode is desired in a PA resonant cell. Thus when choosing either a size or specific resonant frequency, the eigenvalues for the other resonant modes have to be considered. If possible to make sure that the geometry of the PA cell is chosen so that the eigenvalues for the other operating modes are as far away as possible from the desired mode. This should have the side effect of boosting the effective quality of the PA cell.

An approach to designing a PA cell is to build it out of blocks. These blocks can consist of the resonator, high, low or band-pass acoustic filters and buffer volumes. Tavakoli

(2010) along with other authors, who designed their PA cells with analytical methods, extensively use buffer volumes sized to be a quarter wavelength $(\lambda/4)$ to isolate the resonant chamber from external noise at the resonant frequency.

### Transmission line model

The Transmission Line Model (TLM) is a well known and widely used model in the area of photo-acoustic spectroscopy. The principle of transmission line theory is the discretisation of the circuit elements, resistance, capacitance and inductance into a per unit length impedance from which a characteristic impedance and propagation constant is derived (Sadiku, 2007:429-430).

Standing waves are caused by the interference between the incident and reflected waves. This is because the reflected wave goes in and out of phase with the incident wave so maxima and minima are created. Because of these maxima and minima the amplitude of the signal arriving at the load can potentially be unnecessarily diminished or fluctuating depending on the reflection coefficient. The reflection coefficient describes the ratio of the amplitude of the reflected wave to the incident wave. For any system to achieve maximum power transfer from the source to the load the reflection coefficient would be zero (i.e. no reflections). However in an acoustic system a reflection coefficient of 1 would be the perfect result for a resonator (i.e. positive reinforcement of standing wave) and a coefficient of -1 would be best for an acoustic filter as there would be complete destructive interference.

Impedance matching is also a useful design tool where two transmission lines of different characteristic impedances can be joined without loss of power by using a quarter-wavelength $(\lambda/4)$ transformer. Figure 8 is a simplified transmission line representation. It shows the source $V_s$ and it internal impedance $Z_s$ driving a transmission line with a length of $l$, characteristic impedance of $Z_o$ and propagation coefficient of $\gamma$ into a load of $Z_L$ (Sadiku, 2007:423-485).

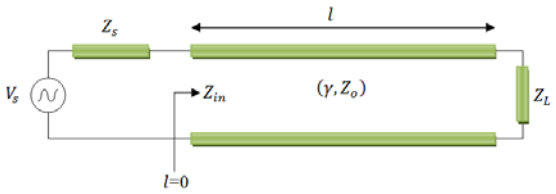


**Figure 8.** Electrical Transmission Line, where the source $V_s$ and it internal impedance $Z_s$ driving a transmission line with a length of $l$, characteristic impedance of $Z_o$ and propagation coefficient of $\gamma$ into a load of $Z_L$.

For the purpose of PA the TLM allows the use of lumped acoustic elements to conceptualise an acoustic system as an electrical transmission line if the wavelength of operation is larger than the dimensions of the PA cell.

### Lumped acoustic elements

Analogous comparison of electrical circuit to acoustic system is shown by Apfel (1998:145). Equations (6) and (7) compare an electrical system to a mechanical system.

$$L\frac{\partial^2 i}{\partial t^2} + R\frac{\partial i}{\partial t} + \frac{1}{C}i = v \tag{6}$$

$$M\frac{\partial^2 x}{\partial t^2} + c\frac{\partial x}{\partial t} + kx = F \tag{7}$$

In (6), $L$ is inductance in Henrys $H$, $R$ is resistance in Ohms $\Omega$, $C$ is capacitance in Farads $F$, $i$ is current in Amperes $A$, $v$ in volts $V$, In (7), $M$ is the mass in $kg$, c is the damping factor in $Nsm^{-1}$, $k$ is the spring constant is $Nm^{-1}$, $F$ is the force in Newtons $(N)$ and $x$ is displacement in metres $(m)$.

By equating the terms of those equations, mechanical systems and acoustic systems alike can be modelled and solved using an electrical circuit analogy. Therefore a basic acoustic system can be modelled as an electrical transmission line. Using these discrete circuit elements as defined by Nordhaus (1981) in equations (8), (9) and (10),

$$R = 8\pi\eta l/A^2 \tag{8}$$

$$L = \rho l/A \tag{9}$$

$$C = V/(v_s^2.\rho) \tag{10}$$

where $R$ is the resistive elements in $kgs^{-1}m^{-2}$, $\eta$ is the viscosity in $kgs^{-1}m^{-1}$, $l$ is the length of discrete element in metres $m$, $A$ is the cross-sectional area of the acoustic element in $m^2$, L is the inductive elements in $kgm^{-4}$, $\rho$ is the mass density in $kgm^{-3}$, $C$ is the capacitive elements in $skg^{-1}m^{-2}$, $V$ is the volume in $m^3$ and $v_s$ is the free-space sound velocity in $ms^{-1}$.

Rey (2004) takes the above equations and applies them to electrical transmission line theory. Obtaining equations (11), (12), (13), (14), (15) and (16),

$$Z_\omega^c = \frac{\rho c}{\pi r_i^2}\sqrt{\frac{1+d_v/r_i}{1+(\gamma-1)d_t/r_i}} \times\left[1-\frac{i}{2}\left(\frac{(\gamma-1)}{r_i/d_v+1}-\frac{(\gamma-1)}{r_i/d_t+(\gamma-1)}\right)\right] \tag{11}$$

$$\gamma_\omega^c = \frac{i\omega}{c}\sqrt{\left(1+\frac{d_v}{r_i}\right)}\left(1+(\gamma-1)\frac{d_t}{r_i}\right) \times\left[1-\frac{i}{2}\left(\frac{(\gamma-1)}{r_i/d_t+(\gamma-1)}+\frac{1}{r_i/d_v}\right)\right] \tag{12}$$

$$Z_{ai} = Z_\omega^c \tanh\left(\frac{\gamma_\omega^c l_i}{2}\right) \tag{13}$$

$$Z_{bi} = \frac{Z_\omega^c}{\sinh(\gamma_\omega^c l_i)} \tag{14}$$

$$d_v = \sqrt{\frac{2\eta}{\rho\omega}} \tag{15}$$

$$d_t = \sqrt{\frac{2K}{\rho\omega C_p}} \tag{16}$$

where $Z_\omega^c$ is the characteristic impedance in $kgm^{-4}s^{-1}$, $\gamma_\omega^c$ is the propagation constant, $Z_{ai}$ is the series component of the discrete acoustic element in $kgm^{-4}s^{-1}$, $Z_{bi}$ is the parallel component of the discrete acoustic element in $kgm^{-4}s^{-1}$, $d_v$ is the thickness of viscous boundary layer in metres $m$, $d_t$ is the thickness of thermal boundary layer in metres $m$, $i$ is the index refering to the different tubes in the system $(i = 1\ to\ 5)$, $r_i$ is the $i^{th}$ tube's radius in metres $m$, $l_i$ is the $i^{th}$ tube's length in metres $m$, $K$ is the thermal conductivity in $Wm^{-1}K^{-1}$, $\gamma$ is the ratio of specific heats (unitless) and $\omega$is the frequency in radians.

The impedance of the discontinuity $Z_{ri}$ caused by the change in diameter between two connected tubes is derived by Karal

(1953) as equation (17) (see Karal (1953) for the discontinuity correction factor $H(r_{min}/r_{max})$),

$$Z_{ri} = i\omega\sqrt{\frac{8\rho}{3\pi^2 r_{min}}}H\left(\frac{r_{min}}{r_{max}}\right) \quad (17)$$

where $r_{min}$ is the radius $(m)$ of the smaller cylinder and $r_{max}$ is the radius $(m)$ of the larger cylinder.

Using equations (11) – (17) and $Z_w = 4 \times 10^6\ kgm^{-4}s^{-1}$ (Rey, 2004), the acoustic impedance of the windows of the cell, a TLM model can be generated as shown in Figure 9 for the cylindrical resonator shown in Figure 10. Using this model the acoustic signal arriving at the microphone is the voltage developed across $I_2$. Standard electrical theory of Superposition and Kirchhoff's voltage and current laws are used to solve for the voltage developed across $I_2$.

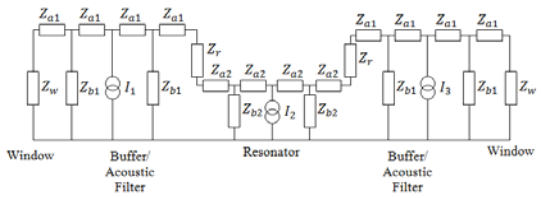


**Figure 9.** A sample TLM model for a simple two buffer volume single tube resonator.

### Photo-acoustic resonant cells

Cylindrical resonators are the most common type of resonators found in photo-acoustic spectroscopy and are primarily longitudinal resonators. They have medium to high quality factors ranging from $Q = 10$ to $Q \geq 250$ (Miklos, 2001) (Liu, 2010). This is because of the use of more than just a resonant cylinder in the PA cell design. The use of $\lambda/4$ buffer volumes is the most extensive, providing acoustic filtering, as shown in Figure 10. The buffer volumes are used by Riddle (2006), Rey, (2004, 2008 & 2010) Schmid (2006) and Tavakoli (2010) to construct mid to high range quality factor PA cells.

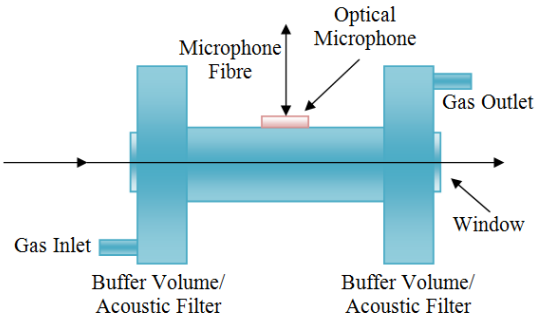


**Figure 10.** Single tube resonator with two buffer volumes.

The design of the PA cell doesn't have to be limited to one resonant cylinder, as Liu (2010) uses a dual resonant cylinder setup to measure at two different resonant frequencies.

The Helmholtz resonator resonates via a different technique by the combination of resonant and non-resonant cells interconnected by a pipe, see Figure 11. The mass of gas in that pipe acts as a piston and the two chambers connected to it act as springs, forming a simple mechanical oscillator. The Helmholtz resonator uses an indirect measuring technique by moving the microphone into another chamber which isn't directly excited by the light source. This design has the advantage of increasing the PA cell noise rejection but it sacrifices the signal amplitude as there are significant losses between the excited and measurement chambers. These losses can be reduced by designing the PA cells with impedance matching in mind. But as a result of the indirect measurement most Helmholtz resonators only have low to mid-low quality factor of $10 \leq Q < 100$ (Miklos, 2001) (Barbier, 2002). Depending on the design and resonant mode used the output signal can be boosted if multiple pipes are used, this increases the amount of power transferred, but unfortunately also increases the amount of noise transferred as well.

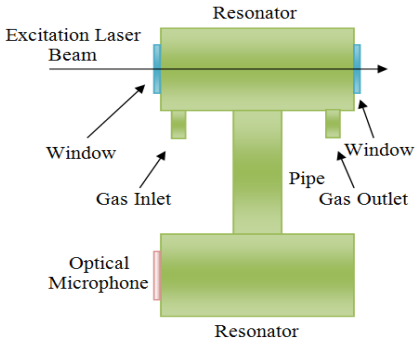


**Figure 11.** Simple twin resonant cell with an interconnecting pipe.

## QUARTZ ENHANCED PHOTO-ACOUSTIC SPECTROSCOPY

Quartz Enhanced Photo-Acoustic Spectroscopy (QEPAS) uses a quartz resonator, typically a 32.768 $kHz$ Quartz Tuning Fork (QTF) used in wrist watches as the transducer in the PA cell. Using a QFT has the advantage of an extremely high quality factor of $Q$~100,000 in a vacuum and $Q$~10,000 in air at 1 $atm$ (Kosterev, 2005). The typical setup for QEPAS is detailed by Kosterev (2005). The typical setup is similar to Figure 12 with the exception of the use of an optical microphone. Instead of the optical microphone the QTF is used as a piezoelectric resonant transducer. To read the concentration the piezoelectric effect of the quartz would be harnessed and electrically amplified to a useful level for instrumentation.

A novel approach to a QEPAS system is shown in Figure 12, where instead of using the piezoelectric effect of the quartz to read the PA signal a Laser Doppler Vibrometer (LDV) is employed. The operation and maths of the LDV is described later in the paper. The LDV indirectly measures the PA signal by measuring the derivative of the displacement (velocity) of the forks as they bend while resonating. The QTF can replace the entire PA cell, but for increased noised immunity the tuning fork can be placed inside of an acoustic filter. The rest of the system functions as the LPAS described in Figure 4, except with the requirement of the laser being pulsed. This is because the PA signal will decrease with modulation frequency, as shown in equation (2).

The novel aspects included in the QEPAS approach are a smaller sensor head, higher immunity to environmental noise, high potential sensitivity and 2f modulation method for background noise elimination (Kosterev, 2005).

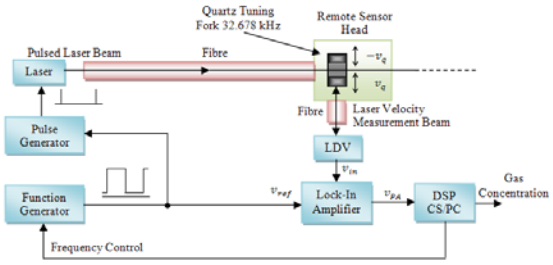


**Figure 12.** Quartz Enhanced Photo-Acoustic Spectroscopy (QEPAS)

### Laser Doppler Vibrometer

The LDV utilises two wave phenomena, the Doppler Effect and beats to modulate the velocity of the QTF onto the laser light. Figure 13 details the operation of the LDV. One path of the laser light ($f_L$) is untouched and is passed straight to the Photo-Detector (PD). The other is phase (frequency) modulated to provide a useful carrier frequency ($f_c$) for the velocity information ($f_r$).

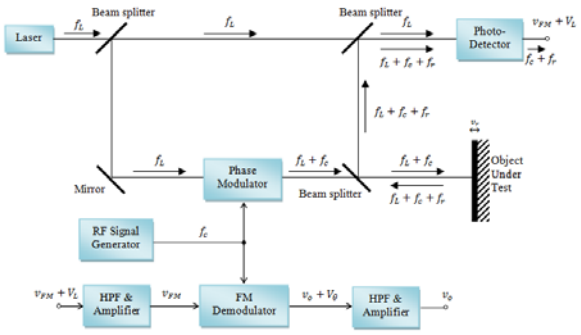


**Figure 13.** LDV (Laser Doppler Vibrometer)

The Doppler Effect is the change in the frequency observed at the receiver because of the source's movement. For the application of an LDV the Doppler Effect is where the source and receiver are stationary and the object under test is moving. A wave is emitted from the source and reflected by the object. The returning wave's frequency is modified by the relative difference in their velocities, as described by equation (18),

$$\Delta f = -\frac{v_s - v_r}{\lambda_0} \tag{18}$$

where $\Delta f$ is the change frequency $(Hz)$ of the reflected wave, $v_s$ is the velocity $(ms^{-1})$ of the emitted wave, $v_r$ is the velocity $(ms^{-1})$ of the object and $\lambda_0$ is the wavelength $(m)$ of the wave from the source. Because the source is stationary $v_s = 0\ ms^{-1}$ equation (18) becomes equation (19),

$$\Delta f = \frac{v_r}{\lambda_0} = f_r \tag{19}$$

where $f_r$ is the frequency of the reflected wave (Goldwasser, 1965).

To retrieve the velocity information the principle of beats are used at the PD. Beats are formed when two sinusoidal waves are summed, the result is an interference pattern with beat frequencies of $|f_2 \pm f_1|$. This is shown by summing two waves, equations (20) and (21) with the result of equation (22) due to trigonometry,

$$y_1 = A_1 cos(2\pi f_1 t), \quad y_2 = A_2 cos(2\pi f_2 t) \tag{20), (21}$$

$$y_1 + y_2 = A_1 cos(2\pi f_1 t) + A_2 cos(2\pi f_2 t)$$

$$y_1 + y_2 = A_2 cos(2\pi (f_1 + f_2)t) cos(2\pi (f_1 - f_2)t)$$

$$+(A_1 - A_2) cos(2\pi f_1 t) \tag{22}$$

where $f_1 = f_L, f_2 = f_L + f_c + f_r$ from Figure 13, $A_1$is the amplitude of the direct laser beam, $A_2$ is the amplitude of the reflected laser beam, $y_1$ is the direct laser beam and $y_2$ is the reflected laser beam (Goldwasser, 1965).

$$y_1 + y_2 = A_2 cos(2\pi (2f_L + f_c + f_r)t) cos(2\pi (f_c + f_r)t)$$

$$+(A_1 - A_2) cos(2\pi f_L t) \tag{23}$$

Because the PD has a limited Bandwidth (BW) it acts as a low-pass filter, where the BW$\ll f_L$, and drops the extremely high frequency components of the light and only keeps the $f_c + f_r$ and Direct-Current (DC) components, which results is equation (24),

$$v_{FM} + V_L = K_{PD}[A_2 cos(2\pi (f_c + f_r)t) + (A_1 - A_2)] \tag{24}$$

where $v_{FM} + V_L$ is the voltage $(V)$ returned from the PD containing the velocity of the QTF as frequency modulated signal and DC component representing most of the direct laser amplitude and $K_{PD}$ is the PD transducing and gain coefficient $(VW^{-1})$.

To eliminate the DC component from the PD a High-Pass Filter (HPF) and amplifier are used to boost the signal enough for the FM demodulator to demodulate the signal. They obtain only the velocity information an additional HPF and amplifier are used to remove the phase error $V_\theta$ and boost the velocity information $v_o$ to a useful amplitude for input into the rest of the system, resulting in the overall equation for the LDV or equation (25),

$$v_o = K_2 K_{FM} K_1 K_{PD} A_2 \frac{v_r}{\lambda_o} \tag{25}$$

where $K_1$ and $K_2$ are the gains of the HPF and amplifiers, $K_{FM}$ is the gain of the FM demodulator circuit, $\lambda_o$ is the wavelength $(m)$ of the LDV laser and $v_r$ is the velocity $(ms^{-1})$ of the QTF.

## CONCLUSION

This paper has presented an approach to intrinsically-safe gas detection using a modulated laser which excites an acoustic resonance in a detection chamber. Advanced modelling of the chamber acoustics is important to both signal maximization and calibration of the overall system. The processing of the acoustic standing-wave measurements from the resonant chamber represents one of the main challenges, and we have described several possible approaches to maximizing the signal-to-noise ratio. The goal of the work is to produce a low-cost sensor which requires minimal expertise to deploy and calibrate.

## REFERENCES

Andersen, Brigid, 2010, 'Mine Disaster Leaves Nation in Mourning', *ABC News*, 24 November 2010, <http://www.abc.net.au/news/2010-11-24/mine-disaster-leaves-nation-in-mourning/2349618>.

Apfel, R 1998, 'Acoustic Lumped Elements From First Principles', in Crocker, M (eds.), *Handbook of Acoustics*, John Wiley & Sons, USA.

Bageshwar, D, Pawar, A, Khanvilkar, V, Kadam, V 2010, 'Photoacoustic Spectroscopy and Its Applications – A Tutorial Review', *Eurasian Journal of Analytical Chemistry*, Vol. 5, No 2, 2010, Pages 187-203.

Bartlome, R, Kaucikas, M & Sigrist, M 2009, 'Modulated resonant versus pulsed resonant photoacoustics in trace gas detection', *Applied Physics B: Lasers and Optics*, Vol. 96, Pages 561-566, viewed 29 April 2011, SpringerLINK, Springer-Verlag.

Bialkowski, S 1996, 'Photothermal Spectroscopy Methods for Chemical Analysis', Vol. 134, in Winefordner, J (eds.), *Chemical Analysis: A Series of Monographs on Analytical Chemistry and its Applications*, John Wiley & Sons, USA.

Brown *et al*, R 2011, "Surat Basin Future Directions Statement", *Surat Basin Future Directions Statement Steering Committee*, report to Queensland State Government, <http://www.regions.qld.gov.au/dsdweb/v4/apps/web/content.cfm?id=15173>.

EPA 2011, 'Natural Gas', *US Environmental Protection Agency*, <http://www.epa.gov/cleanenergy/energy-and-you/affect/natural-gas.html>.

Goldwasser, E 1965, '*OPTICS, WAVES, ATOMS, AND NUCLEI: An Introduction'*, W. A. Benjamin, New York.

Horowitz, P and Hill, W 1990, 'Ch 15.5 Lock-In Detection', *The Art of Electronics*, Cambridge University Press, Cambridge, UK.

Karal, F 1953, 'The Analogous Acoustical Impedance for Discontinuities and Constrictions of Circular Cross Section', *Journal of the Acoustical Society of America*, Vol. 25, Pages 327-324, viewed 5 April 2011, Acoustic Society of America.

Kosterev, A, Tittel, F, Serebryakov, D, Malinovsky, A and Morozov, I 2005, '', *Review of Scientific Instruments*, Vol. 76, viewed 2 June 2011, SpringerLINK, Springer-Verlag.

Liu, W, Wang, L, Li, L, Liu, J, Liu, F and Wang, Z 2010, 'Fast simultaneous measurement of multi-gases using quantum cascade laser photoacoustic spectroscopy', *Applied Physics B: Lasers and Optics*, Vol. 103, No. 3, Pages 743-747, viewed 4 April 2011, SpringerLINK, Springer-Verlag.

L'vov, B 1970, *Atomic Absorption Spectrochemical Analysis*, Adam Hilger, London.

McKenna, P 2011, 'Thousands of gas leaks under Boston and San Francisco', *New Scientist*, viewed 6 July 2011, <http://www.newscientist.com/article/mg21128203.800-thousands-of-gas-leaks-under-boston-and-san-francisco.html>.

Miklos, A, Hess, P & Bozoki, Z 2001, 'Application of acoustic resonators in photoacoustic trace gas analysis and metrology', *Review of Scientific Instruments*, Vol. 72, Pages 1937-1955, viewed 19 July 2011, SpringerLINK, Springer-Verlag.

Ngai, A, Persijn, S, Von Basum, G and Harren, F 2006, 'Automatically tunable continuous-wave optical parametric oscillator for high-resolution spectroscopy and sensitive trace-gas detection', *Applied Physics B: Lasers and Optics*, Vol. 85, Pages 173-180, viewed 1 March 2011, SpringerLINK, Springer-Verlag.

Nordlhaus, N & Pelzl, J 1981, 'Frequency Dependence of resonant Photoacoustic Cells: The Extended Helmholtz Resonator', *Applied Physics A: Materials Science & Processing*, Vol. 25, Issue 3, Pages 221-229, viewed 29 April 2011, SpringerLINK, Springer-Verlag.

Polson, J & Klimasinska, K 2010, 'PG&E Gas Line Blast Kills at Least Four, Destroys 38 Homes', viewed 29 September 2010, <http://www.bloomberg.com/news/2010-9-10/gas-explosion-in-san-francisco-suburb-kills-at-least-four-destroys-houses.html >.

Preston, D and Deitz, E 1991, 'Appendix A: Modulation Spectroscopy: The Lock-In Amplifier', *The Art of Experimental Physics*, John Wiley & Sons, New York.

Rey, J and Sigrist, W 2008, 'Simultaneous dual-frequency excitation of a resonant photoacoustic cell', *Infrared Physics & Technology*, Vol. 51, Pages 516-519, viewed 1 March 2011, Elsevier, ScienceDirect.

Rey, J, Romer, C, Gianella, M and Sigrist, M 2010, 'Near-infrared resonant photoacoustic gas measurement using simultaneous dual-frequency excitation', *Applied Physics B: Lasers and Optics*, Vol. 100, Pages 189-194, viewed 1 March 2011, SpringerLINK, Springer-Verlag.

Riddle, A & Selker, M 2006, 'Impedance-optimized photoacoustic spectroscopy', *Applied Physics B: Lasers and Optics*, Vol. 85, Pages 329-336, viewed 29 April 2011, SpringerLINK, Springer-Verlag.

Sadiku, M 2007, *Elements of Electromagnetics*, 4th edn., Oxford University Press, New York.

Sasada, H 1996, 'Near-Infrared Molecular Spectroscopy and Possible Frequency References for Frequency Control of Semiconductor Lasers', in Ohtsu, M (eds.), *Frequency Control of Semiconductor Lasers*, John Wiley & Sons, New York.

Schilt, S, Besson, J and Thevenaz, L 2006, 'Near-infrared laser photoacoustic detection of methane: the impact of molecular relaxation', *Applied Physics B: Lasers and Optics*, Vol. 82, Pages 319-329, viewed 29 April 2011, SpringerLINK, Springer-Verlag.

Schmid, T 2005, 'Photoacoustic spectroscopy for process analysis', *Analytical and Bioanalytical Chemistry*, Vol. 384, Pages 1071-1086, 29 April 2011, SpringerLINK, Springer-Verlag.

Sigrist, M 2002, 'Trace gas monitoring by laser photoacoustic spectroscopy and related techniques (plenary)', *Review of Scientific Instruments*, Vol. 74, No. 1, Pages 486-490, viewed 2 March 2011, SpringerLINK, Springer-Verlag.

Sigrist, M, Marinov, D, Vogler, D & Rey, J 2004, 'Investigation and optimisation of a multipass resonant photoacoustic cell at high absorption levels', *Applied Physics B: Lasers and Optics*, Vol. 80, Pages 261-266, viewed 4 April 2011, SpringerLINK, Springer-Verlag.

Slezak, V 2003, 'Signal processing in pulsed photoacoustic detection of trace by means of a fast Fourier transform-based method', *Review of Scientific Instruments*, Vol. 74, Issue 1, Pages 642-644, viewed 2 March 2011, SpringerLINK, Springer-Verlag.

*Spectroscopy of Atmospheric Gases* 2011, Spectropic and absorption line interactive database compiled from HITRAN data of atmospheric gases, Russian Foundation For Basic Research, viewed 14 March 2011, <http://spectra.iao.ru/en/>.

Stevenson, A 2010, 'New Blast: All Miners Feared Dead', *Sydney Morning Herald*, viewed 24 November 2010, <http://www.smh.com.au/world/new-blast-all-miners-feared-dead-20101124-1862p.html>.

Tavakoli, M, Tavakoli, A, Taheri, M and Saghafifar, H 2010, 'Design, simulation, and structural optimization of a longitudinal acoustic resonator for trace gas detection using laser photoacoustic spectroscopy (LPAS)', *Optics & Laser Technology*, Vol. 42, Pages 828-838, viewed 6 June 2011, Elsevier, ScienceDirect.